15

Heat Transfer Performances and Exergetic Optimization for Solar Heat Receiver

Jian-Feng Lu[1] and Jing Ding
School of Engineering,
Sun Yat-sen University,
China

1. Introduction

Solar energy is one kind of important resource for clean and renewable energy, and is widely investigated in many fields. In order to increase the operating temperature and thermodynamic efficiency, concentrated solar radiation is widely used to heat the working fluid in solar thermal power system (Trieb & Nitsch, 1998) and other industrial engineerings (Klein et al., 2007; Ali et al., 2008). Concentrated solar radiation (Kalogirou, 2004) can be collected by the parabolic trough collector, parabolic dish reflector, heliostat field, etc. The concentrated energy flux has been studied in kinds of solar energy system. Moustafa et al. (1995) measured the solar flux density distribution on a plane receiver due to a flat heliostat. Estrada et al. (2007) proposed a calorimeter to measure the concentrated solar power produced by a point focus solar concentrator.

Solar thermal power system based on trough, dish or heliostat field is a very promising and challenging technology for its high operating temperature and thermodynamic efficiency. In solar thermal power plant (Odeh et al., 2003), the heat transfer medium in solar heat receiver is heated by concentrated solar radiation to some high temperature, and then it can be used to operate kinds of heat engine and generate electricity. As a result, the heat receiver (Ortega et al., 2008) is the key problem for the photo-thermal transformation, and the heat transfer performance of solar heat receiver is the hotspot for solar energy research. The basic types of heat receiver in concentrated solar thermal system mainly include heat pipe receiver (Fujiwara et al., 1990), parabolic trough solar receiver (Gong et al., 2010), cavity receiver (Wu et al., 2010), and multistage solar receiver (Taragan, 1999), etc.

The dynamical and thermal characteristics of solar heat receiver have been investigated in much literature (Cui et al., 2008; Grena, 2010). In general, the heat losses from solar receiver mainly include three contributions: radiation heat loss, convective heat loss, and conduction heat loss. The radiation heat loss (Melchior et al., 2008; Li et al., 2010) is mainly dependent upon the receiver structure, wall temperature, and emissivity/absorptivity of the receiver walls, while the convective heat loss (Clausing, 1981) is mainly determined by the receiver structure, wall temperature, and wind velocity. The heat conduction loss (Zavoico, 2001) exists in cavity receiver through the insulation wall, and it can be ignored in many solar heat receivers.

[1] Corresponding author

In order to reduce the radiation heat loss, solar selective coatings are widely used in solar heat receiver. Tabor (1958) first reported the solar selective coating to increase the absorption efficiency of solar heat receiver. The ideal solar selective coating was considered to have good optical performance with high absorptivity and low emissivity. Kennedy (2002) introduced kinds of solar selective coatings under mid- to high-temperature conditions. Cindrella (2007) studied the real utility ranges of the solar selective coatings. Nilsson & Roos (2009) further evaluated the optical and thermal properties of coatings for energy efficient windows. In general, solar selective coatings mainly have six types: intrinsic coatings, semiconductor-metal tandems, multilayer coatings, multi-dielectric composite coatings, textured surfaces, and selectively solar-transmitting coatings. Intrinsic coatings are not effective enough but very stable, like metallic W (Agnihotri & Gupta, 1981), CaF_2 (Pellegrini, 1980), SnO_2 (Seraphin & Meinel, 1976) etc. Semiconductor-metal tandems as Si-based design can be used in a wide temperature range (Seraphin, 1976). Multilayer coatings (Andersson et al., 1980) can be very efficient for proper structure design. Metal-dielectric composite coatings (Arancibia et al., 2000; Gao et al., 2000) have a high absorptivity in the solar region, while that is transparent in the other region. Till now, solar selective coatings have been critical important topic for solar energy research.

The convective heat loss (Siebers & Kraabel, 1984) is normally very difficult to determine but very important for the total energy loss of solar heat receiver. Clausing (1983) predicted the convective loss from solar central receivers from analytical model and experimental result. LeQuere et al. (1981a, 1981b) experimentally reported Nusselt number correlations for isothermal open cubical cavity for different inclination. Koenig & Marvin (1981) investigated convective heat loss in open cavity solar receivers, and proposed a calculating model in a large operating temperature range. Chan & Tien (1985, 1986) studied the laminar natural convection in shallow open cavities. Leibfried & Ortjohann (1995) investigated convective heat loss from upward and downward facing cavity receivers, and analyzed the effects of wall temperature, tilt angle, aperture-radius, geometry, ribs, and ventilation. Khubeiznet et al. (2002) measured natural convection heat transfer from an isothermal hemispherical cavity. Taumoefolau et al. (2004) described the convective loss from electrically heated cavity receiver under different inclinations and temperatures. Paitoonsurikarn et al. (2006) simulated the convective loss from solar cylindrical receiver and dish concentrating receiver. Sendhil & Reddy (2007, 2008) carried out numerical analyses of convective losses in rectangular, hemispherical solar cavity receiver and modified cavity receivers, respectively. In addition, the convective loss from heat receiver under wind condition is also investigated. Ma (1993) reported the experimental investigations on the convective loss under wind.

Available literature also investigated combined heat loss from solar heat receiver including convection and radiation. Lage et al. (1992) simulated natural convection and radiation in a 2-D cavity with open end. McDonald (1995) reported the heat loss from an open cavity including convection and radiation. Dehghan & Behnia (1996) numerically studied combined natural convection conduction and radiation heat transfer in a discretely heated open cavity. Reddy & Kumar (2008) investigated the combined laminar natural convection and surface radiation heat transfer in a modified cavity receiver of solar parabolic dish. Prakash et al. (2009) investigated the heat losses from a solar cavity receiver, and found the natural convection and radiation played the premier role in the heat loss of the receiver. Muftuoglu & Bilgen (2008) simulated heat transfer in inclined rectangular receivers for concentrated solar radiation.

The optimal structure design and operating conditions of solar heat receiver have also been investigated by various methods. Harris & Lenz (1985) found the thermal and optical losses from a cavity solar receiver were less than other types of receiver. Kaushika and Reddy (2000) designed the modified cavity receiver to perform minimum heat loss from the receiver with

fuzzy focal dish concentrators. Steinfeld & Schubnell (1993) investigated the solar cavity receiver, and educed the optimum aperture size and operating temperature by a semi empirical method. Segal & Epstein (2003) analyzed the optimized working temperatures of a solar central receiver. Kongtragool & Wongwises (2005) provided a theoretical analysis on the optimum absorber temperature of a once-reflecting full conical concentrator for maximizing the overall efficiency of a solar-powered low temperature differential Stirling engine.

Some researchers began to analyze the exergy transfer of solar collector and receiver. Bejan et al. (1981) considered the solar collector systems using second law analysis and synthesis. Singh et al. (2000) carried out the basic energy and exergetic analysis for typical solar thermal power systems to evaluate the respective losses as well as exergetic efficiency under given operating conditions. Farahat et al. (2009) developed an exergetic optimization method of flat plate solar collectors to determine the optimal performance and design parameters of these solar thermal energy conversion systems. Till now, few researchers theoretically investigated the heat and exergy transfer performances of solar heat receiver combined with forced convection and solar selective coating effects in detail.

The objective of this chapter is to report the heat and exergy transfer characteristics of solar heat receiver under unilateral concentrated solar radiation based on our group's research works. The heat and exergy transfer model coupling of forced convection inside the receiver and heat loss outside the receiver is first established, and the heat absorption performances are calculated under different heat transfer media, solar selective coatings, incident energy fluxes, inlet temperatures and velocities, and receiver structure. In addition, the uneven heat transfer characteristics on the receiver surface are described due to the unilateral concentrated solar radiation, and the exergetic efficiency of solar heat receiver is optimized under kinds of operating condition.

2. Physical model and exergetic analyses of solar heat receiver

2.1 Physical model for solar heat receiver

To simplify solar heat receiver in solar thermal power system, a straight pipe with solar selective coating is demonstrated as illustrated in Fig. 1. For theoretical investigation, the thickness and thermal resistance of the pipe wall are ignored. In practical solar thermal power system, the heat receiver is usually a cavity (Hogan et al., 1990) or evacuated tube (Li & Wang, 2006) and the heat losses of the natural convection and radiation can be reduced corresponding to that of the pipe receiver. As a result, the absorption efficiency of the pipe receiver is lower than that of cavity receiver or evacuated tube, but it does not affect its basic heat transfer performances under different heat transfer media, solar selective coatings, incident energy fluxes, inlet temperatures and velocities, and receiver pipe radii.

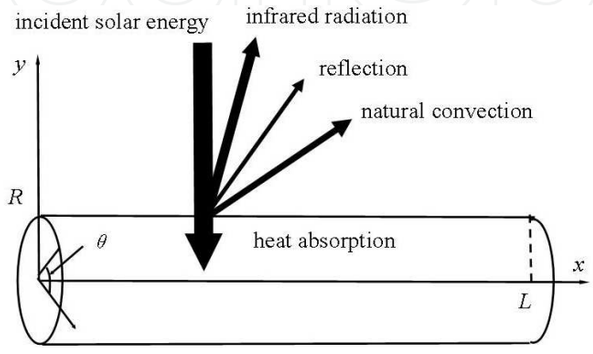

Fig. 1. The physical model of heat transport in solar heat receiver

The incident energy is directly concentrated by solar collector system, and its energy flux density can be calculated by $I_0 = C\kappa_0 I_s$, here C means concentration ratio, κ_0, the reflectivity of the collector system, I_s, solar energy flux. The incident energy flux on the receiver wall can be expressed as:

$$I = I_0 \sin\theta \qquad \text{for } \sin\theta \geq 0 \tag{1a}$$

$$I = 0 \qquad \text{for } \sin\theta < 0 \tag{1b}$$

The energy flux directly absorbed by solar heat receiver is only aI for the reflective effect, here a means the absorptivity of solar selective coating. The natural convection outside the receiver plays an important role in the heat loss, and its heat transfer coefficient is assumed to be h_n. At high temperature, the infrared radiation heat loss is very significant, and it can be calculated as $\varepsilon\sigma(T_w^4 - T_s^4)$, here T_w means the receiver temperature, ε is the emissivity of solar selective coating. Beside the optical reflection and heat losses, the incident energy is used to increase the inner energy of the working fluid. According to the previous analyses, the energy conservation equation can be expressed as (Lu et al., 2010a):

$$\alpha I = h_n(T_w - T_s) + \varepsilon \cdot \sigma\left(T_w^{\,4} - T_s^{\,4}\right) + q_f \tag{2}$$

where T_s denotes the environment temperature, q_f means the convective heat flux inside the receiver, and this equation has a good agreement with that derived by Kongtragool & Wongwises (2005).

The convective heat flux inside the receiver can be calculated as:

$$q_f = h_f \cdot \left(T_w - T_f\right) \tag{3}$$

where $$T_f = \frac{\int_0^R \rho c_p u T 2\pi r dr}{\int_0^R \rho c_p u 2\pi r dr},\ h_f = Nu \cdot \frac{k}{D}.$$

For fully developed turbulent flow inside the receiver, the Nusselt number can be correlated as (Lienhard IV & Lienhard V, 2002):

$$Nu = 0.0243\,Re^{0.8}\,Pr^{0.4} \tag{4}$$

Substituting Eq. (3) into Eq. (2) yields

$$\alpha I = h_n(T_w - T_s) + \varepsilon \cdot \sigma\left(T_w^{\,4} - T_s^{\,4}\right) + h_f\left(T_w - T_f\right) \tag{5}$$

The local wall temperature can be directly derived from Eq. (5), and the energy transport along the flow direction is:

$$\int_0^{2\pi} q_f \cdot R d\theta = \rho c_p \frac{\partial}{\partial x}\int_0^{2\pi}\int_0^R uT \cdot r dr d\theta = \rho c_p \frac{\partial T_f}{\partial x} \cdot \pi R^2 u_{av} \tag{6}$$

where T_f and u_{av} means the average fluid temperature and flow velocity.

2.2 Heat absorption and exergetic efficiency of heat receiver

The local heat absorption efficiency can be described as:

$$\eta_{ab} = \frac{q_f}{I} = \frac{h_f\left(T_w - T_f\right)}{I} \tag{7}$$

From Eq. (7), the absorption efficiency for a certain circumference can be calculated as:

$$\overline{\eta_{ab}} = \frac{\int_0^{2\pi} q_f R d\theta}{I_0 \cdot 2R} \tag{8}$$

From Eq. (8), the absorption efficiency of the whole receiver is:

$$\overline{\overline{\eta_{ab}}} = \frac{\int_0^L \int_0^{2\pi} q_f(x) \cdot R d\theta dx}{I_0 \cdot 2RL} = \frac{\int_0^L \overline{\eta_{ab}} dx}{L} \tag{9}$$

Integrating Eq. (6) yields

$$\int_0^x \int_0^{2\pi} q_f \cdot R d\theta dx' = \int_0^x \rho c_p \frac{\partial T_f}{\partial x'} \cdot \pi R^2 u_{av} dx' \tag{10}$$

From Eq. (10), the inner energy increment due to heat absorption along the flow direction is

$$\Delta E(x) = \int_0^x \int_0^{2\pi} q_f \cdot R d\theta dx' = \rho c_p \cdot \pi R^2 u_{av} \cdot \left(T_f - T_{f0}\right) \tag{11}$$

where T_{f0} is the inlet fluid temperature.

Exergy is defined as the maximum amount of work which can be produced by a system or a flow of matter or energy as it comes to equilibrium with a reference environment (Kotas, 1995). In solar thermal power system, the electricity generation in the turbine cycle is directly determined by the exergy increment in the heat receiver. Since concentrated solar heat flux density is high enough, the pressure loss can be normally ignored in exergetic analyses, and the exergy flow at a certain place of solar receiver will be:

$$\dot{E} = \rho c_p \cdot \pi R^2 u_{av} \cdot \left[T_f - T_s - T_s \ln\left(\frac{T_f}{T_s}\right) \right] \tag{12}$$

The exergy flow increment along the flow direction is:

$$\Delta \dot{E}(x) = \dot{E}(x) - \dot{E}(0) = \rho c_p \cdot \pi R^2 u_{av} \cdot \left[T_f - T_{f0} - T_s \ln\left(\frac{T_f}{T_{f0}}\right) \right] \tag{13}$$

From Eqs. (11) and (13), the exergetic efficiency of the absorbed energy is:

$$\eta_{ex,ab} = \frac{\delta \Delta \dot{E}}{\delta \Delta E} = \frac{\partial \Delta \dot{E} / \partial T_f \cdot \delta T_f}{\partial \Delta E / \partial T_f \cdot \delta T_f} = 1 - \frac{T_s}{T_f} \tag{14}$$

Obviously, the exergetic efficiency of the absorbed energy is just equal to the Carnot efficiency. From Eqs. (8) and (14), the exergetic efficiency of the incident energy flux is:

$$\eta_{ex} = \overline{\eta_{ab}}\eta_{ex,ab} \tag{15}$$

The exergetic efficiency of the whole heat receiver (Lu et al., 2010b) is:

$$\overline{\eta_{ex}} = \frac{\Delta \dot{E}(L)}{I_0 \cdot 2RL} = \frac{1}{L} \cdot \int_0^L \eta_{ex} dx \tag{16}$$

2.3 Caculation parameters

The heat transfer media in solar thermal power plant mainly include water/steam (Zarza et al., 2004), molten salts (Reilly & Kolb, 2001) and air (Bai, 2010), etc. In order to analyze the heat transfer performance of solar heat receiver in detail, the heat transfer media are assumed to be Hitec heat transfer salt and air in present article. If the air is used as the heat transfer medium at high temperatures, it can replace natural gas in a gas turbine with high thermodynamic efficiency. In addition, Hitec heat transfer salt can also be used in a wide temperature range.

Though the properties of heat transfer media and solar selective coatings are normally temperature dependent, the temperature non-dependent parameters of heat transfer media and coatings are helpful for theoretical analyses. The properties of Hitec heat transfer salt (Brenntag Company) and air (Lienhard IV & Lienhard V, 2002) are assumed to be constant at the reference temperature of 573 K and atmospheric pressure, and their associated parameters are presented in Table 1. The radiation parameters of solar selective coatings (Cindrella, 2007) are illustrated in Tables 2.

Properties	Hitec heat transfer salt	Air
ρ	1862 kgm^{-3}	1.77 kgm^{-3}
c_p	1510 $Jkg^{-1}K^{-1}$	1006 $Jkg^{-1}K^{-1}$
k	0.571 $Wm^{-1}K^{-1}$	0.0181 $Wm^{-1}K^{-1}$
μ	0.0030 $kgm^{-1}s^{-1}$	0.0000134 $kgm^{-1}s^{-1}$

Table 1. Properties of Hitec heat transfer salt and air (T_{ref}=573 K, P_{ref}=1 atm)

Material	a	ε	a/ε
Co-Cd-BT	0.96	0.12	8
Pyromark	0.93	0.83	1.12

Table 2. Radiation parameters of solar selective coatings

The heat transfer coefficient of natural convection h_n is 5.0 $Wm^{-2}K^{-1}$, and the environment temperature T_s=293 K. Besides, the basic geometrical parameters of solar heat receiver are assumed to be R=0.010 m.

3. Local heat transfer performances of heat receiver

3.1 Heat transfer performances with different heat transfer media

According to previous analyses, the local wall temperature and absorption efficiency can be directly derived from Eqs. (5) and (7). Fig. 2 illustrates the wall temperature and absorption

efficiency of heat receiver with Pyromark coating with different heat transfer media, where T_f=523 K, u_{av}=5.0 ms^{-1}. As the incident energy flux rises, the wall temperature almost linearly increases, while the absorption efficiency will first increase and then decrease. The wall temperature of molten salts receiver will reach 736.09 K at the incident energy flux of 2.5 MWm^{-2}, while the wall temperature of air receiver reaches as high as 768.2 K only at the incident energy flux of 30 kWm^{-2}. In addition, the local absorption efficiency of molten salts receiver reaches its maximum 92.46% at optimal incident energy flux of 2.0 MWm^{-2}, while that of air receiver will reach its maximum 32.08% at optimal incident energy flux of 18 kWm^{-2}.

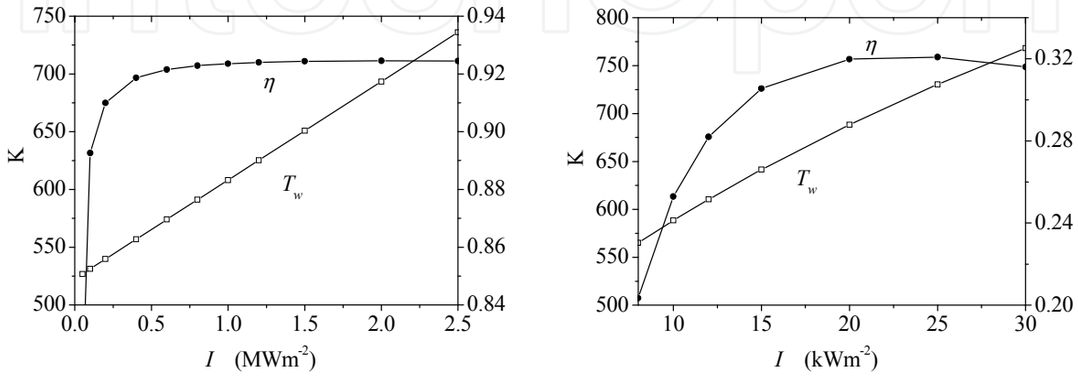

(a) Molten salts (b) Air

Fig. 2. Heat transfer characteristics with different heat transfer media (T_f=523 K, u_{av}=5.0 m/s)

In general, the heat transfer characteristics of heat receiver with molten salts and air are very similar under different incident energy fluxes, but the absorption efficiency and optimal incident energy flux of molten salts receiver are significantly higher than those of air receiver. As a result, the solar selective coating will play more important role in air receiver, because its absorption efficiency can change in a large range.

3.2 Basic heat transfer performances under different solar selective coatings

Since solar selective coating is critical important in air receiver, the heat transfer performances of air receiver will be further studied with different solar selective coatings in this section.

Fig. 3 presents the wall temperature and absorption efficiency of air receiver with different solar selective coatings, where T_f=523 K, u_{av}=5.0 ms^{-1}. Apparently, the wall temperature with high emissivity as Pyromark will be lower than that with low emissivity as Co-Cd-BT. At low incident energy flux, the wall temperature almost linearly increases with the incident energy flux, and then its increasing rate will drop a little at high incident energy flux. In general, the absorption efficiency will reach maximum at optimal incident energy flux. Since the incident energy flux I is dependent upon the solar energy flux, incident angle and concentrator ratio, the concentrator ratio will have an optimal value due to Fig. 3b. In addition, solar selective coatings with low emissivity can obviously increase the energy absorption efficiency. For the receiver with Pyromark, the heat absorption efficiency is only about 30.5%, so it is not a good coating material for air receiver. For the receiver with low emissivity as Co-Cd-BT, the local absorption efficiency can reach its maximum 64.2% with incident energy flux of 15 kWm^{-2}.

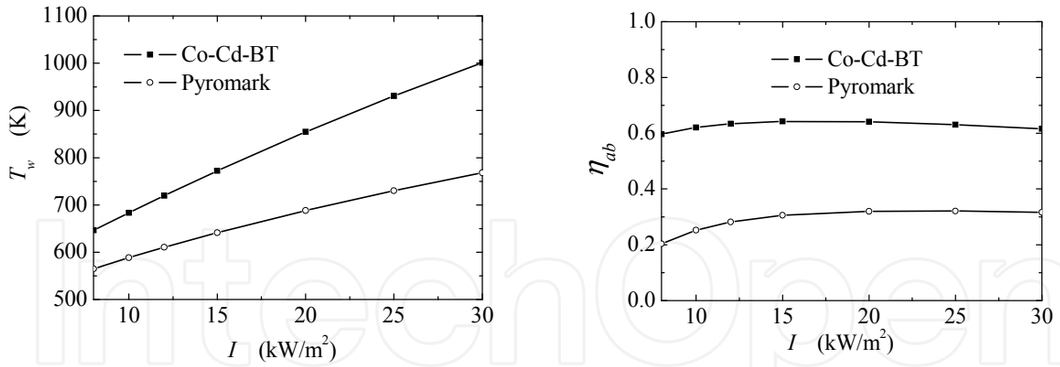

(a) The wall temperature (b) Absorption efficiency

Fig. 3. Heat transfer characteristics with different solar selective coatings (T_f=523 K, u_{av}=5.0 ms^{-1})

Fig. 4 further describes the energy percentage distribution during the absorption process of air receiver with different solar selective coatings, where T_f=523 K, u_{av}=5.0 ms^{-1}. As the incident energy flux rises, the energy percentage of the reflection keeps constant, while the energy percentage of natural convection significantly decreases. The energy percentage of radiation loss will first decrease at low incident energy flux, and then it increases at higher incident energy. Because of the natural convection and radiation, the heat absorption efficiency will first increase and then decrease with the incident energy flux, and it has a maximum at optimal incident energy flux. For air receiver with high emissivity, the radiation loss is much higher than that with low emissivity, so the heat absorption efficiency is very low.

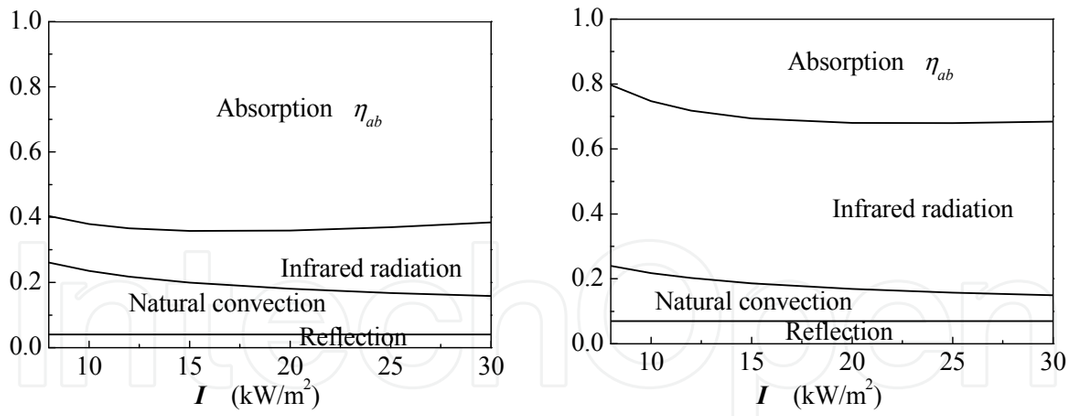

(a) Co-Cd-BT (b) Pyromark

Fig. 4. The energy percentage distribution during the heat absorption process (T_f=523 K, u_{av}=5.0 ms^{-1})

Fig. 5 presents the heat losses of natural convection and radiation from the receiver wall. As the wall temperature increases from 400 K to 1000 K, the heat loss of natural convection linearly increases from 1.07 kWm^{-2} to 7.07 kWm^{-2}, the radiation heat loss for Co-Cd-BT jumps from 0.17 kWm^{-2} to 6.08 kWm^{-2}, while the radiation heat loss for Pyromark jumps from 1.20 kWm^{-2} to 47.06 kWm^{-2}. As a conclusion, solar selective coating plays the principal role in the heat loss at high temperature.

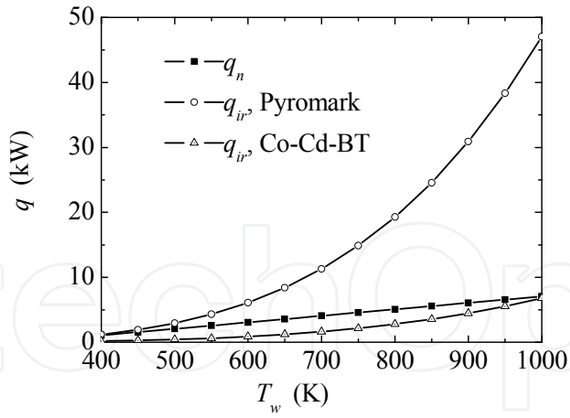

Fig. 5. The heat losses of natural convection and radiation from the receiver wall

Apparently, the absorption efficiency of the cavity receiver and glass envelope with vacuum will be higher than that of solar pipe receiver here, because the heat loss is reduced by the receiver structure, but the basic heat absorption performances with different incident energy flux, coating material, and other conditions are very similar. In order to simply the description, only air receiver with Co-Cd-BT and molten salts receiver with Pyromark will be considered in the following investigation.

3.3 Heat transfer performances with different parameters

Fig. 6 presents the heat transfer characteristics of molten salts receiver with different pipe radii, where T_f=473 K, u_{av}=1.0 ms^{-1}, R=0.010 m, 0.008 m, and 0.006 m. In any other descriptions, the radius of receiver pipe is only assumed to be 0.010 m. As the pipe radius decreases, the heat transfer coefficient of forced convection inside the pipe rises, so the heat absorption efficiency will also rise with the wall temperature dropping. When the pipe radius is reduced from 0.010 m to 0.006 m, the maximum heat absorption efficiency will be increased from 90.95% to 91.14%, and the optimal incident energy flux changes from 0.6 MWm^{-2} to 0.8 MWm^{-2}. As a conclusion, the heat absorption efficiency normally varies slowly with the pipe radius, because the thermal resistance of forced convection inside the pipe is normally very little.

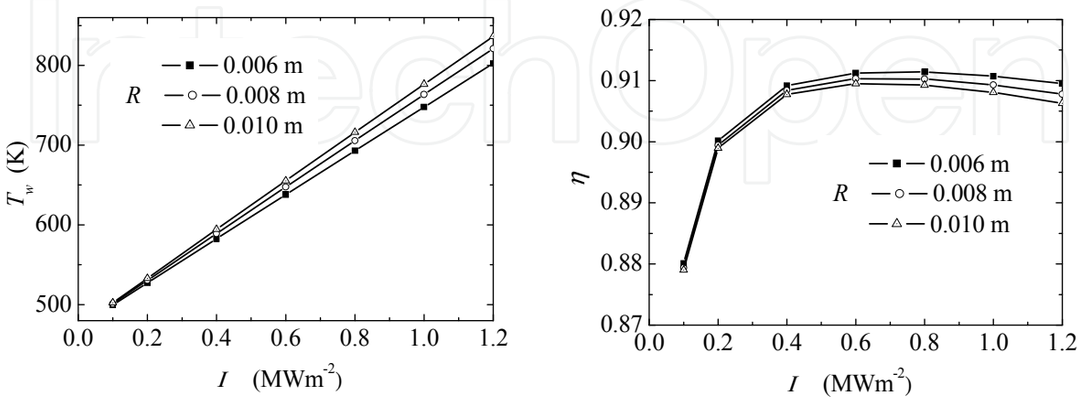

(a) The wall temperature (b) The local absorption efficiency

Fig. 6. Heat transfer performances of molten salts receiver with different pipe radii (T_f=473 K, u_{av}=1.0 ms^{-1})

The heat transfer characteristics of molten salts receiver with different flow velocities are described in Fig. 7, where T_f=473 K, u_{av}=0.5 ms^{-1}, 1.0 ms^{-1}, and 2.0 ms^{-1}. When the flow velocity increases, the heat absorption efficiency significantly rises with the wall temperature dropping, because the heat convection inside the receiver is obviously enhanced. When the inlet velocity rises from 0.5 ms^{-1} to 2.0 ms^{-1}, the wall temperature under incident energy flux 1.0 MWm^{-2} will drop from 984.3 K to 649.2 K, while the maximum heat absorption efficiency increases from 89.49% to 91.82%, and the optimal incident energy flux also changes from 0.4 MWm^{-2} to 1.2 kWm^{-2}. As a result, the heat transfer performance of the receiver can be remarkably promoted with the flow velocity rising.

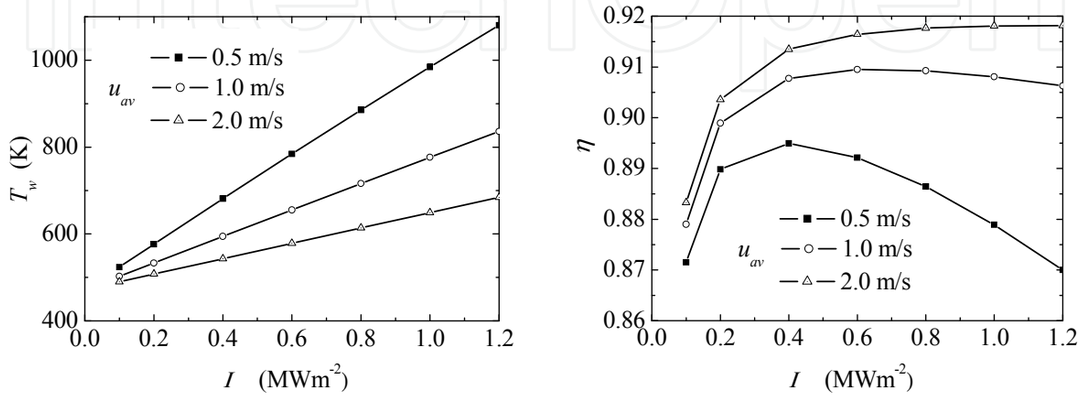

(a) The wall temperature (b) The local absorption efficiency

Fig. 7. Heat transfer performances of molten salts receiver with different flow velocities (T_f=473 K)

The wall temperature and absorption efficiency under different fluid temperature are presented in Fig. 8, where I=0.40 MWm^{-2}, u_{av}=1.0 ms^{-1}. As the bulk fluid temperature rises, the wall temperature almost linearly increases, while the absorption efficiency accelerating decreases. As the bulk fluid temperature changes from 350 K to 800 K, the heat absorption efficiency will be reduced from 91.96% to 83.83%.

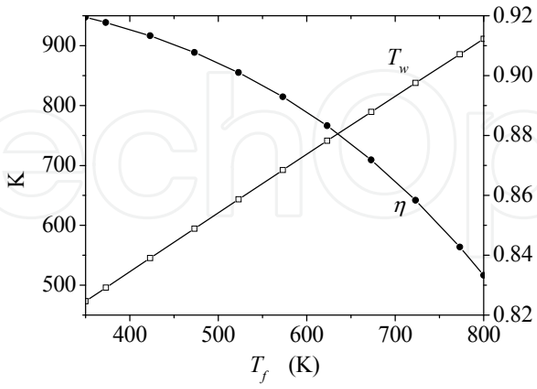

Fig. 8. Heat transfer performances of molten salts receiver with different fluid temperatures (I=0.40 MWm^{-2}, T_f=473 K)

In general, the local absorption efficiency of solar receiver increases with the flow velocity, but decreases with the receiver radius and fluid temperature, and that of air receiver is similar.

4. Uneven heat transfer characteristics along the pipe circumference

Since the incident energy flux is quite different along the receiver pipe circumference, the circumferential heat transfer performance is expected to be uneven. Fig. 9a presents the incident and absorbed energy fluxes along the circumference of molten salts receiver, where I_0=0.40 MWm^{-2}, T_f=473 K, u_{av}=1.0 ms^{-1}, 0≤θ≤90^o. As the angle θ increases from the parallelly incident region (θ=0^o) to the perpendicularly incident region (θ=90^o), the absorbed energy flux increases with the incident energy flux, and their difference or the heat loss including natural convection and radiation also significantly increases. On the surface without incident energy or sin θ<0, the energy flux is -0.0041 MWm^{-2}, and that is just equal to the heat loss outside the pipe wall.

Fig. 9b further illustrates the wall temperature and absorption efficiency along the circumference of molten salts receiver, where I_0=0.40 MWm^{-2}, T_f=473 K, u_{av}=1.0 ms^{-1}, 0≤θ≤90^o. Apparently, the wall temperature first linearly increases with the angle θ, then increases slowly near the perpendicularly incident region, and the maximum temperature difference along the circumference is 122.69 K. When the incident energy flux increases with the angle θ, the absorption efficiency will first rises sharply, and then it approaches to the maximum 90.78% in the perpendicularly incident region. In the region without incident energy or sin θ<0, the wall temperature is 471.63 K, while the absorption efficiency is negative infinitely great for zero incident energy flux.

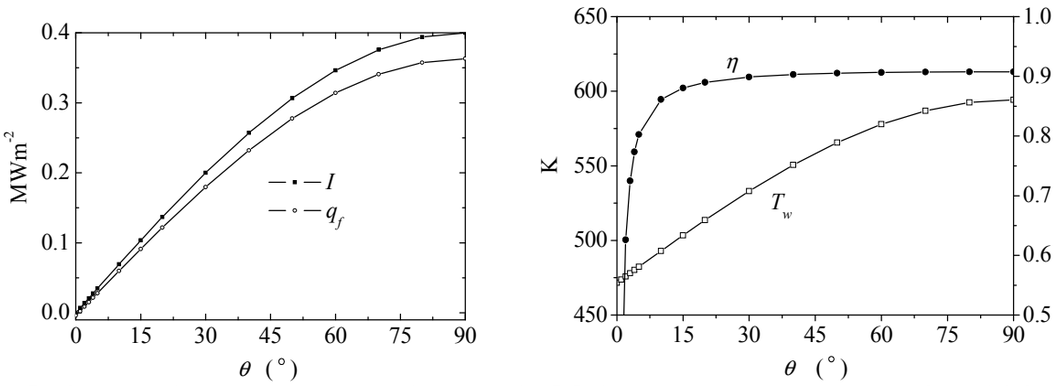

(a) Incident and absorbed energy fluxes (b) Wall temperature and absorption efficiency

Fig. 9. Incident and absorbed energy fluxes along the circumference of molten salts receiver (I_0=0.40 MWm^{-2}, T_f=473 K, u_{av}=1.0 ms^{-1})

In addition, the average incident energy flux, wall temperature and absorption efficiency of the circumference 0≤θ≤360^o can be described as:

$$\bar{I} = \frac{\int_0^{\pi} I(\theta)\cdot R d\theta}{2\pi R} = \frac{2RI_0}{2\pi R} = \frac{I_0}{\pi} \tag{17a}$$

$$\overline{T_w} = \frac{\int_0^{2\pi} T_w(\theta)\cdot R d\theta}{2\pi R} = \frac{\int_0^{2\pi} T_w(\theta)\cdot d\theta}{2\pi} \tag{17b}$$

$$\overline{\eta_{ab}} = \frac{\int_0^{2\pi} q_f(\theta)\cdot R d\theta}{I_0\cdot 2R} = \frac{\int_0^{2\pi} q_f(\theta) d\theta}{2I_0} \tag{17c}$$

Parameters	nomenclature	value	uncertainty
Heat flux	$\bar{I}$	0.127 MWm^{-2}	0
Temperature	$\overline{T_w}$	510.61 K	0.16 K
	$T_w(\bar{I})$	510.77 K	
Absorption efficiency	$\overline{\eta_{ab}}$	88.63%	0.15%
	$\eta_{ab}(\bar{I})$	88.78%	

Table 3. The average and calculated heat transfer parameters of molten salts receiver (I_0=0.40 MWm^{-2}, T_f=473 K, u_{av}=1.0 ms^{-1})

The average parameters of the whole circumference of molten salts receiver are illustrated in Table 3, where I_0=0.40 MWm^{-2}, T_f=473 K, u_{av}=1.0 ms^{-1}. From Eqs. (5) and (7), the wall temperature and absorption efficiency corresponding to the average incident energy flux can be directly derived, and the results are also presented in Table 3. As a result, the heat transfer parameters calculated from the average incident energy flux has a good agreement with the average parameters of the whole circumference, and the uncertainties of the wall temperature and absorption efficiency are 0.16 K and 0.15%, respectively.

Furthermore, the wall temperature, incident and absorbed energy fluxes along the circumference of air receiver are presented in Fig. 10, where I_0=20 kWm^{-2}, T_f=473 K, u_{av}=10 ms^{-1}, $0 \le \theta \le 90^o$. As the angle θ increases, the wall temperature and absorbed energy flux both significantly increases with the incident energy flux. In the perpendicularly incident region, the wall temperature and absorbed energy flux approach maximums of 772.15 K and 14.38 kWm^{-2}. In the region without incident energy or sin θ<0, only heat loss appears.

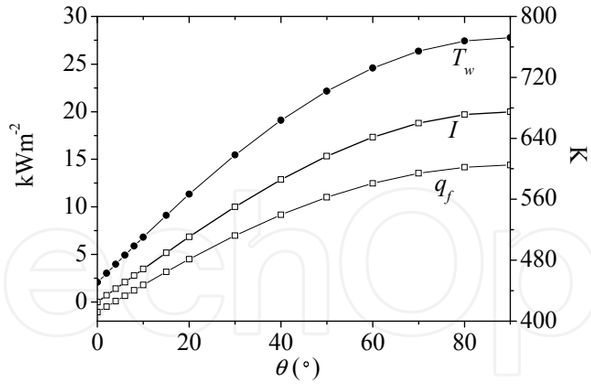

Fig. 10. Heat transfer performances along the pipe circumference of air receiver (T_f=473 K, u_{av}=10 ms^{-1}, I_0=20 kWm^{-2})

Table 4 illustrates the average heat transfer parameters of the whole circumference of air receiver, where T_f=473 K, u_{av}=10 ms^{-1}, I_0=20 kWm^{-2}. Obviously, the heat transfer parameters of air receiver calculated from the average incident energy flux also has a good agreement with the average parameters of the whole circumference, and the uncertainties of the wall temperature and absorption efficiency are respectively 4.04 K and 1.9%, which are larger than those of molten salts receiver.

Parameters	nomenclature	value	uncertainty
Heat flux	$\bar{I}$	6.37 kWm^{-2}	0
Temperature	$\overline{T_w}$	554.64 K	4.04 K
	$T_w(\bar{I})$	558.68 K	
Absorption efficiency	$\overline{\eta_{ab}}$	62.8%	1.9%
	$\eta_{ab}(\bar{I})$	64.7%	

Table 4. The average and calculated heat transfer parameters of air receiver (T_f=473 K, u_{av}=10 ms^{-1}, I_0=20 kWm^{-2})

In general, the average absorption efficiency along the whole circumference of molten salt receiver or air receiver is almost equal to the absorption efficiency corresponding to the average incident energy flux, and then

$$\int_0^{2\pi} q_f \cdot R d\theta = 2\pi R\bar{I} \cdot \bar{\eta} \approx 2\pi R\bar{I} \cdot \eta(\bar{I}) = 2\pi R \cdot q_f(\bar{I}) \tag{18}$$

5. Heat transfer and absorption performances of the whole receiver

In order to investigate the heat transfer performance of the whole receiver, the energy transport equation along x direction from Eqs. (6) and (18) is derived as:

$$\int_0^{2\pi} q_f \cdot R d\theta = \rho c_p \frac{\partial}{\partial x}\int_0^R Tu(r) \cdot 2\pi r dr = \rho c_p \frac{\partial T_f}{\partial x}\pi R^2 u_{av} \tag{19}$$

Substituting Eq. (18) into Eq. (19) yields

$$2\pi R \cdot q_f(\bar{I}) = \rho c_p \frac{\partial T_f}{\partial x}\pi R^2 u_{av} \tag{20}$$

Eq. (20) can be simplified as:

$$\frac{\partial T_f}{\partial x} = \frac{2q_f(\bar{I})}{\rho c_p R u_{av}} \tag{21}$$

Fig. 11 presents the heat transfer and absorption characteristics of molten salts receiver along the flow direction, where I_0=0.40 MWm^{-2}, T_{f0}=473 K. Apparently, the bulk fluid temperature and average wall temperature almost linearly increase along the flow direction. For higher flow velocity, the temperature difference of the fluid and wall is lower for higher heat transfer coefficient, and the temperature gradient along the flow direction is also smaller. As the flow velocity increases from 0.5 ms^{-1} to 2.0 ms^{-1}, the average wall temperature in the outlet drops from 821.5 K to 574.0 K, and that can remarkably benefit the receiver material. The heat absorption efficiency of the receiver will be larger for high flow velocity, and the heat absorption efficiency in the outlet rises from 72.01% to 86.77% as the flow velocity increasing from 0.5 ms^{-1} to 2.0 ms^{-1}.

The heat transfer and absorption characteristics of air receiver along the flow direction is further described in Fig. 12, where I_0=31.4 kWm^{-2}, T_{f0}=523 K, u_{av}=5.0 ms^{-1}. Along the flow direction, the temperatures of fluid and wall increases, while the heat absorption

efficiency decreases very quickly. As a result, the temperature and absorption characteristics of air receiver along the flow direction is very similar to those of molten salts receiver, and only heat transfer performances of molten salts receiver will be described in detail in this section.

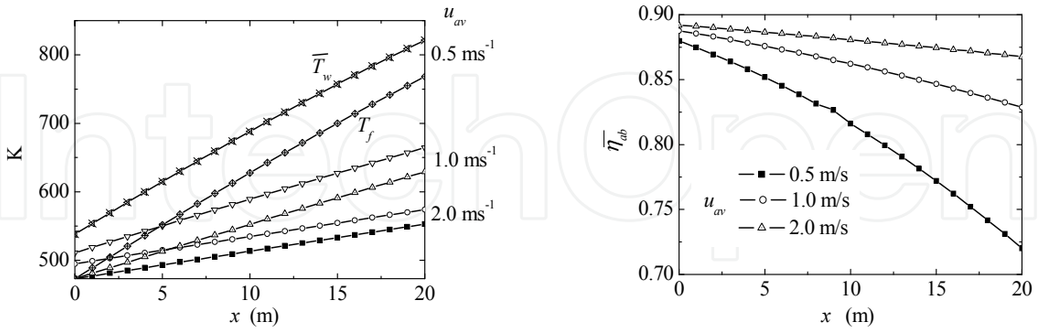

(a) The wall and fluid temperatures (b) The local absorption efficiency

Fig. 11. The heat transfer and absorption characteristics of molten salts receiver along the flow direction (I_0=0.40 MWm^{-2}, T_{f0}=473 K)

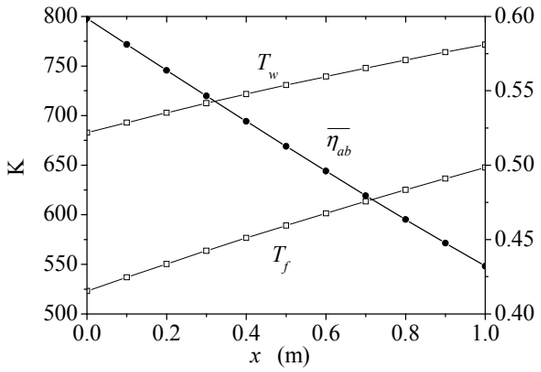

Fig. 12. The heat transfer and absorption characteristics of air receiver along the flow direction (I_0=31.4 kWm^{-2}, T_{f0}=523 K)

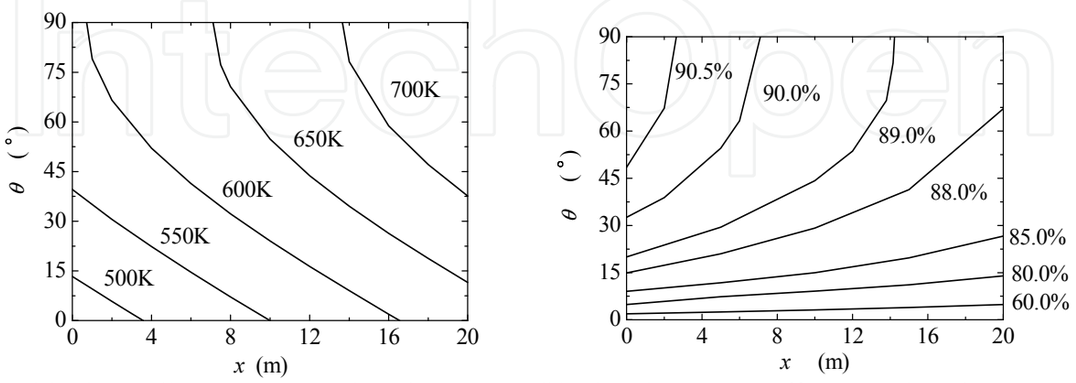

(a) The wall temperature distribution (b) The absorption efficiency distribution

Fig. 13. The temperature and absorption efficiency distributions of the whole receiver (I_0=0.40 MWm^{-2}, T_{f0}=473 K, u_{av}=1.0 ms^{-1})

Fig. 13 illustrates the wall temperature and absorption efficiency distributions of molten salt receiver in detail, where I_0=0.40 MWm^{-2}, T_{f0}=473 K, u_{av}=1.0 ms^{-1}. Apparently, the wall temperature increases with the angle θ and along the flow direction, and the maximum temperature difference of the receiver wall approaches to 274 K. The isotherms periodically distributes along the flow direction, and they will be normal to the receiver axis near the perpendicularly incident region. Additionally, the absorption efficiency increases with the angle θ, but it decreases along the flow direction with the fluid temperature rising. In general, the absorption efficiency in the main region is about 85-90%, and only the absorption efficiency near the parallelly incident region is below 80%. These results have a good agreement with molten salts receiver efficiency for Solar Two (Pacheco & Vant-hull, 2003).

Fig. 14a further presents the average absorption efficiency of the whole molten salts receiver with different flow velocities and lengths, where I_0=0.40 MWm^{-2}, T_{f0}=473 K. As the receiver length increases, the average absorption efficiency of the receiver drops with the fluid temperature rising. When the receiver length increases from 5.0 m to 20 m, the average heat absorption efficiency of the receiver with the flow velocity of 1.0 ms^{-1} drops from 88.19% to 86.09%. As the flow velocity increases, the average absorption efficiency of the whole receiver significantly rises for enhanced heat convection. When the flow velocity increases from 0.5 ms^{-1} to 2.0 ms^{-1}, the average heat absorption efficiency of the receiver of 20 m will rise from 81.07% to 88.05%.

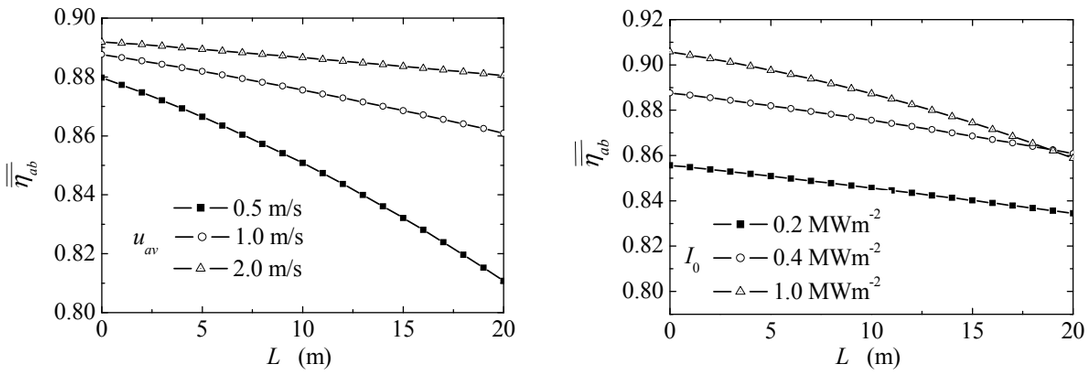

(a) Different velocities (I_0=0.40 MWm^{-2}) (b) Different energy fluxes (u_{av}=1.0 ms^{-1})

Fig. 14. The average absorption efficiency of molten salts receiver (T_{f0}=473 K)

Fig. 14b describes the average absorption efficiency of the whole molten salts receiver with different concentrated solar fluxes, where T_{f0}=473 K, u_{av}=1.0 ms^{-1}. For higher concentrated solar flux, the average heat absorption efficiency of the receiver with small length is higher, but its decreasing rate corresponding to the length is also higher. As the receiver length is 20 m, the efficiency of the receiver with 1.0 MWm^{-2} is lower than that with 0.4 MWm^{-2}, because the absorption efficiency drops with the wall temperature rising. When the concentrated solar flux is increased from 0.2 MWm^{-2} to 1.0 MWm^{-2}, the average heat absorption efficiency for the receiver of 20 m will rise from 83.45% to 85.87%.

6. Exergetic optimization for solar heat receiver

According to the previous analyses, the heat absorption efficiency of air receiver changes much more remarkably than that of molten salts receiver, so the air receiver will be considered as an example to investigate the energy and exergy variation in this section.

Fig. 15 illustrates the inner energy and exergy flow increments and incident energy derived from Eqs. (11) and (13), where I_0=31.4 kWm^{-2}, T_{f0}=523 K, u_{av}=5.0 ms^{-1}. Along the flow direction, the incident energy linearly increases, while the increasing rate of the inner energy flow drops with the absorption efficiency decreasing. On the other hand, the exergy flow are dependent upon the absorption efficiency and fluid temperature. For the whole receiver, the inner energy and exergy flow increments and incident energy will be 344.1 W, 171.2 W, and 628.3 W, respectively.

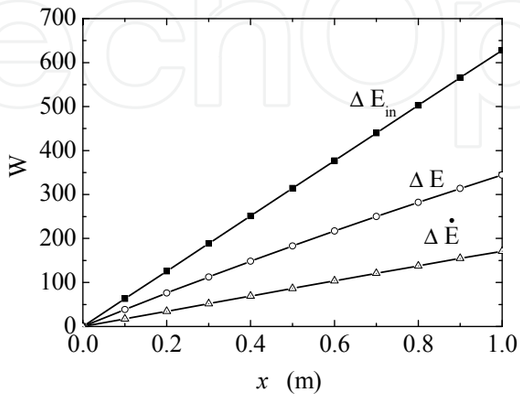

Fig. 15. The inner energy and exergy flow increments and incident energy power (I_0=31.4 kWm^{-2}, T_{f0}=523 K, u_{av}=5.0 ms^{-1})

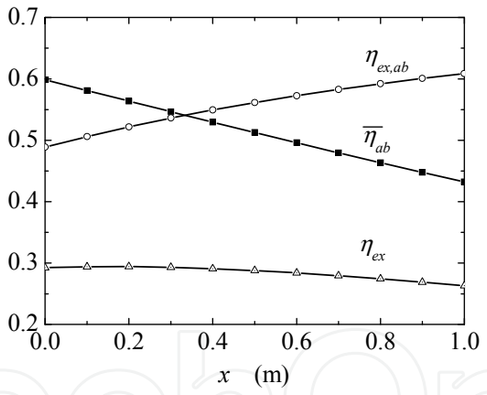

Fig. 16. The heat absorption and exergetic efficiencies of air receiver (I_0=31.4 kWm^{-2}, T_{f0}=523 K, u_{av}=5.0 ms^{-1})

Fig. 16 further presents the heat absorption and exergetic efficiencies along the flow direction, where I_0=31.4 kWm^{-2}, T_{f0}=523 K, u_{av}=5.0 ms^{-1}. Apparently, the heat absorption efficiency almost linearly drops along the flow direction, while the exergetic efficiency of the absorbed energy significantly increases with the fluid temperature rising. Since the exergetic efficiency of incident energy is the product of heat absorption efficiency and exergetic efficiency of the absorbed energy, it will first increase and then decrease along the flow direction. At 0.30 m, the exergetic efficiency reaches its maximum 27.6%, and the corresponding heat absorption efficiency and exergetic efficiency of the absorbed energy are respectively 57.5% and 48.0%. Generally, the exergetic efficiency of incident energy changes just a little along the flow direction, and the average exergetic efficiency of the receiver is 27.3%.

Fig. 17 describes the heat absorption and exergetic efficiencies of air receiver under different concentrated energy fluxes, where I_0=31.4 kWm^{-2} and 47.1 kWm^{-2}, u_{av}=5.0 ms^{-1}. In general, the heat absorption efficiency of heat receiver quickly drops with the inlet temperature, and its decreasing rate under high concentrated energy flux is remarkably larger. Because the exergetic efficiency form absorbed energy decreases with the heat absorption efficiency, the exergetic efficiency of the receiver will first increase and then decrease with the inlet temperature. As the concentrated energy flux increases from 31.4 kWm^{-2} to 47.1 kWm^{-2}, the exergetic efficiency of incident energy increases for about 1.5%-3.0%. At the inlet temperature of 523 K, the exergetic efficiency of the receiver approaches to maximum, and the maximum exergetic efficiencies under incident energy flux of 31.4 kWm^{-2} and 47.1 kWm^{-2} are respectively 27.25% and 28.77%.

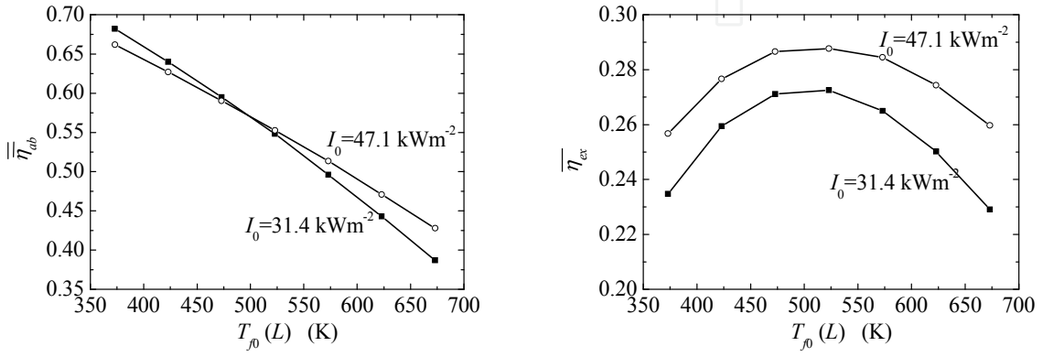

(a) The absorption efficiency (b) The exergetic efficiency

Fig. 17. The absorption and exergetic efficiencies of air receiver with different incident energy fluxes (u_{av}=5.0 ms^{-1})

Fig. 18 futher describes the heat absorption and exergetic efficiencies of air receiver under different flow velocities, where I_0=31.4 kWm^{-2}, u_{av}=3.0 ms^{-1}, 5.0 ms^{-1}, 10.0 ms^{-1}. Apparently, the heat absorption efficiency of air receiver decreases with the inlet temperature rising and flow velocity decreasing. As the inlet temperature rises, the exergetic efficiency of the receiver will reach maximum at optimal inlet temperature. In additional, the maximum exergetic efficiency of incident energy and optimal inlet temperature both increase with flow velocity, and the maximum exergetic efficiencies with flow velocities of 3.0 ms^{-1}, 5.0 ms^{-1} and 10.0 ms^{-1} are respectively 24.45%, 27.25% and 30.95%.

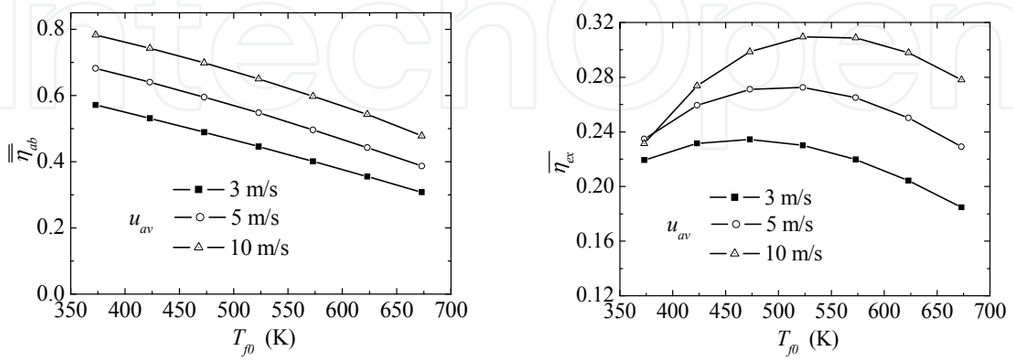

(a) The absorption efficiency (b) The exergetic efficiency

Fig. 18. The absorption and exergetic efficiencies of air receiver with different flow velocities (I_0=31.4 kWm^{-2})

7. Conclusion

The chapter mainly reported the energy and exergetic transfer performances of solar heat receiver under unilateral concentrated solar radiation. The energy and exergetic transfer model coupling of forced convection inside the receiver and heat loss outside the receiver are established, and associated heat transfer characteristics are analyzed under different heat transfer media, solar coating, incident energy flux, inlet flow velocity and temperature, and receiver structure. The absorption efficiency and optimal incident energy flux of heat receiver with molten salts are significantly higher than that with air, and they can be increased by the solar selective coating with low emissivity. As the incident energy flux increases, the energy percentage of natural convection evidently decreases, while the energy percentage of radiation loss will increase at high incident energy flux, so the energy absorption efficiency can reach its maximum at the optimal incident energy flux. As the receiver radius decreasing or flow velocity rising, the heat transfer coefficient of the heat convection inside the receiver increases, and then the heat absorption efficiency can be enhanced. Because of the unilateral concentrated solar radiation and incident angle, the heat transfer is uneven along the circumference, and the absorption efficiency will first sharply rise and then slowly approach to the maximum from the parallelly incident region to the perpendicularly incident region. In the whole receiver, the absorption efficiency of the perpendicularly incident region at the inlet approaches to the maximum, and only the absorption efficiency near the parallelly incident region is low. Along the flow direction, the heat absorption efficiency of the receiver almost linearly decreases, while the exergetic efficiency of the absorbed energy significantly increases, so the exergetic efficiency of incident energy will first increase and then decrease. The exergetic efficiency of the receiver will reach maximum under optimal inlet temperature, and it can be increased with flow velocity rising.

8. Acknowledgements

This chapter is supported by National Natural Science Foundation of China (No. 50806084, No. 50930007) and National Basic Research Program of China (973 Program) (No. 2010CB227103).

9. References

Agnihotri, O. P. & Gupta, B. K. (1981). *Solar Selective Surfaces*. Wiley-Interscience Pub, ISBN 978-047-1060-35-2, New York

Ali, A. H.; Noeres, P. & Pollerberg, C. (2008). Performance assessment of an integrated free cooling and solar powered single-effect lithium bromide-water absorption chiller . *Solar Energy*, Vol. 82, pp. 1021-1030, ISSN 0038-092X

Andersson, A.; Hunderi, O. & Granqvist, C. G. (1980). Nickel pigmented anodic aluminum oxide for selective absorption of solar energy. *Journal of Applied Physics*, Vol. 51, pp. 754-764, ISSN 1089-7550

Arancibia, B. C. A.; Estrada, C. A. & Ruiz-Suárez, J. C. (2000). Solar absorptance and thermal emittance of cermets with large particles. *Journal of Physics D: Applied Physics*, Vol. 33, pp. 2489-2492, ISSN 1361-6463

Bai, F. W. (2010). One dimensional thermal analysis of silicon carbide ceramic foam used for solar air receiver. *International Journal of Thermal Sciences*, Vol. 49, pp. 2400-2404, ISSN 1290-0729

Bejan, A., Keary, D. W. & Kreith, F. (1981). Second law analysis and synthesis of solar collector systems. *Journal of Solar Energy Engineering*, Vol. 103, pp. 23-28, ISSN 0199-6231

Brenntag Company. *Hitec heat transfer salt*. pp. 3-10, Houston. Available from http://www.coal2nuclear.com/MSR%20-%20HITEC%20Heat%20Transfer%20Salt.pdf

Chan, Y. L. & Tien, C. L. (1985). A numerical study of two-dimensional laminar natural convection in shallow open cavities. *International Journal of Heat and Mass Transfer*, Vol. 28, pp. 603-612, ISSN 0017-9310

Chan, Y. L. & Tien, C. L. (1986). Laminar natural convection in shallow open cavities. *ASME Journal of Heat Transfer*, Vol. 108, pp. 305-309, ISSN 0022-1481

Cindrella, L. (2007). The real utility ranges of the solar selective coatings. *Solar Energy Materials and Solar Cells*, Vol. 91, pp. 1898-1901, ISSN 0927-0248

Clausing, A. M. (1981). An analysis of convective losses from cavity solar central receiver. *Solar Energy*, Vol. 27, pp. 295-300, ISSN 0038-092X

Clausing, A. M. (1983). Convective losses from cavity solar receivers - comparisons between analytical predictions and experimental results. *Journal of Solar Energy Engineering*, Vol. 105, pp. 29-33, ISSN 0199-6231

Cui, H. T.; Xing, Y. M.; Guo, Y. S.; Wang, Z. H.; Cui, H. C. & Yuan, A. G. (2008). Numerical simulation and experiment investigation on unit heat exchange tube for solar heat receiver. *Solar Energy*, Vol. 82, pp. 1229-1234, ISSN 0038-092X

Dehghan, A. A. & Behnia, M. (1996). Combined natural convection conduction and radiation heat transfer in a discretely heated open cavity. *ASME Journal of Heat Transfer*, Vol. 118, pp. 54-56, ISSN 0022-1481

Estrada, C. A.; Jaramillo, O. A.; Acosta, R. & Arancibia, B. C. A. (2007). Heat transfer analysis in a calorimeter for concentrated solar radiation measurements. *Solar Energy*, Vol. 81, pp. 1306-1313, ISSN 0038-092X

Farahat, S.; Sarhaddi, F., & Ajam, H. (2009). Exergetic optimization of flat plate solar collectors. *Renewable Energy*, Vol. 34, pp. 1169-1174, ISSN 0960-1481

Fujiwara, M.; Sano, T.; Suzuki, K. & Watanabe, S. Y. (1990). Thermal analysis and fundamental tests heat pipe receiver for solar dynamic space system. *Journal of Solar Energy Engineering*, Vol. 112, pp. 177-182, ISSN 0199-6231

Gao P.; Meng L. J.; Santos M. P.; Teixeira V. & Andritschky M. (2000). Characterization of ZrO_2 films prepared by rf magnetron reactive sputtering at different O2 concentrations in the sputtering gases. *Vacuum*, Vol. 56, pp. 143-148, ISSN 0042-207X

Gong, G. J.; Huang, X. Y.; Wang, J. & Hao M. L. (2010). An optimized model and test of the China's first high temperature parabolic trough solar receiver. *Solar Energy*, Vol. 84, pp. 2230-2245, ISSN 0038-092X

Grena, R. (2010). Optical simulation of a parabolic solar trough collector. *International Journal of Sustainable Energy*, Vol. 29, pp. 19-36, ISSN 1478-646X

Hogan, R. E.; Diver, R. B. & Stine, W. B. (1990). Comparison of a cavity solar receiver numerical model and experimental data. *Journal of Solar Energy Engineering*, Vol. 112, pp. 183-190, ISSN 0199-6231

Kalogirou, S. A. (2004). Solar thermal collectors and applications. *Progress in Energy and Combustion Science*, Vol. 30, pp. 231-295, ISSN 0360-1285

Kaushika, N. D. & Reddy, K. S. (2000). Performance of a low cost solar paraboloidal dish steam generating system. *Energy Conversion and Management*, Vol. 41, pp. 713-726, ISSN 0196-8904

Kennedy, C. E. (2002). *Review of mid- to high-temperature solar selective absorber materials*. NREL/TP-520-31267

Khubeiz, J. M.; Radziemska, E. & Lewandowski, W. M. (2002). Natural convective heat transfers from an isothermal horizontal hemisphericalcavity. *Applied Energy*, Vol. 73, pp. 261-275, ISSN 0306-2619

Klein, H. H.; Karni, J.; Ben-Zvi, R. & Bertocchi, R. (2007). Heat transfer in a directly irradiated solar receiver/reactor for solid-gas reactions . *Solar Energy*, Vol. 81, pp. 1227-1239, ISSN 0038-092X

Koenig, A. A. & Marvin, M. (1981). Convection heat loss sensitivity in open cavity solar receivers, final report. *DOE Contract*, No. EG77-C-04-3985

Kongtragool, B. & Wongwises, S. (2005). Optimum absorber temperature of a once reflecting full conical concentrator of a low temperature differential Stirling engine. *Renewable Energy*, Vol. 30, pp. 1671-1687, ISSN 0960-1481

Kotas, T. J. (1995). *The exergy method of thermal plant analysis*. Malabar, FL: Krieger Publish Company, ISBN 978-089-4649-41-7

Lage, J. L., Lim, J. S. & Bejan, A. (1992). Natural convection with radiation in a cavity with open top end. *ASME Journal of Heat Transfer*, Vol. 114, pp. 479-486, ISSN 0022-1481

Leibfried, U. & Ortjohann, J. (1995). Convective heat loss from upward and downward facing cavity receivers: measurements and calculations. *Journal of Solar Energy Engineering*, Vol. 117, pp. 75–84, ISSN 0199-6231

LeQuere, P.; Penot, F. & Mirenayat, M. (1981a). Experimental study of heat loss through natural convection from an isothermal cubic open cavity. *Sandia Laboratory Report*, SAND81-8014

LeQuere, P.; Humphrey, J. A. C. & Sherman, F. S. (1981b). Numerical calculation of thermally driven two-dimensional unsteady laminar flow in cavities of rectangular cross section. *Numerical Heat Transfer*, Vol. 4, pp. 249-283, ISSN 1521-0634

Li, M. & Wang, L. L. (2006). Investigation of evacuated tube heated by solar trough concentrating system. *Energy Conversion and Management*, Vol. 47, pp. 3591-3601, ISSN 0196-8904

Li, X.; Kong, W. Q.; Wang, Z. F.; Chang, C. & Bai, F. W. (2010). Thermal model and thermodynamic performance of molten salt cavity receiver. *Renewable Energy*, Vol. 35, pp. 981-988, ISSN 0960-1481

Lienhard, IV J. H., Lienhard, V J. H. (2002). *A Heat Transfer Textbook*. Phlogiston Press, Chambridge, ISBN 978-048-6479-31-6, Massachusetts, U.S.A

Lu, J. F.; Ding, J. & Yang, J. P. (2010a). Heat transfer performance of the receiver pipe under unilateral concentrated solar radiation. *Solar Energy*, Vol. 84, pp. 1879-1887, ISSN 0038-092X

Lu, J. F.; Ding, J. & Yang, J. P. (2010b). Heat transfer performance and exergetic optimization for solar receiver pipe. *Renewable Energy*, Vol. 35, pp. 1477-1483, ISSN 0960-1481

Ma, R. Y. (1993). Wind effects on convective heat loss from a cavity receiver for a parabolic concentrating solar collector. *Sandia National Laboratories Report*, SAND92-7293

McDonald, C. G. (1995). Heat loss from an open cavity. *Sandia National Laboratories Report*, SAND95-2939

Melchior, T.; Perkins, C.; Weimer, A. W. & Steinfeld, A. (2008). A cavity-receiver containing a tubular absorber for high-temperature thermochemical processing using concentrated solar energy. *International Journal of Thermal Sciences*, Vol. 35, pp. 981-988, ISSN 1290-0729

Moustafa, M.; Kadry, A. & Ornar M. (1995). Measurements of solar flux density distribution on a plane receiver due to a flat heliostat. *Solar Energy*, Vol. 54, pp. 403-411, ISSN 0038-092X

Muftuoglu, A. & Bilgen, E. (2008). Heat transfer in inclined rectangular receivers for concentrated solar radiation. *International Communications in Heat and Mass Transfer*, Vol. 35, pp. 551-556, ISSN 0735-1933

Nilsson, A. M. & Roos, A. (2009). Evaluation of optical and thermal properties of coatings for energy efficient windows. *Thin Solid Films*, Vol. 517, pp. 3173-3177, ISSN 0040-6090

Odeh, S. D.; Behnia, M. & Morrison, G. L. (2003). Performance evaluation of solar thermal electric generation systems. *Energy Conversion and Management*, Vol. 44, pp. 2425-2443, ISSN 0196-8904

Ortega, J. I.; Burgaleta, J. I. & Téllez F. M. (2008). Central receiver system solar power plant using molten salt as heat transfer fluid. *Journal of Solar Energy Engineering*, Vol. 130, pp. 024501-1-6, ISSN 0199-6231

Pacheco, J. E. & Vant-hull, L. L. (2003). Final results and operating experience of the Solar Two Project. *Advances in solar energy* Vol. 15, pp. 43-81, ISBN 978-184-4072-44-6

Paitoonsurikarn, S. & Lovegrove, K. (2006). A new correlation for predicting the free convection loss from solar dish concentrating receivers. *Proceedings of 44th ANZSES conference*, ISBN 978-097-5065-04-4, Australia

Pellegrini, G. (1980). Experimental methods for the preparation of selectively absorbing textured surfaces for photothermal solar conversion. *Solar Energy Materials*, Vol. 3, pp. 391-404, ISSN 0927-0248

Prakash, M.; Kedare, S. B. & Nayak, J. K. (2009). Investigations on heat losses from a solar cavity receiver. *Solar Energy*, Vol. 83, pp. 157-170, ISSN 0038-092X

Reddy, K. S. & Kumar N. S. (2008). Combined laminar natural convection and surface radiation heat transfer in a modified cavity receiver of solar parabolic dish. *International Journal of Thermal Sciences*, Vol. 47, pp. 1647-1657, ISSN 1290-0729

Reilly, H. E. & Kolb, G. J. (2001). An evaluation of molten-salt power towers including results of the solar two project. *Sandia National Laboratories Report*, SAND2001-3674

Segal, A & Epstein, M. (2003). Optimized working temperatures of a solar central receiver. *Solar Energy*, Vol. 75, pp. 503-510, ISSN 0038-092X

Sendhil, K. N. & Reddy, K. S. (2007). Numerical investigations of natural convection heat loss in modified cavity receiver for fuzzy focal solar dish. *Solar Energy*, Vol. 81, pp. 846-855, ISSN 0038-092X

Sendhil, K. N. & Reddy, K. S. (2008). Comparison of receivers for solar dish collector system. *Energy Conversion and Management*, Vol. 49, pp. 812-819, ISSN 0196-8904

Seraphin, B. O. & Meinel, A. B. (1976a). *Optical Properties of Solids: New Developments*. North Holland Publishing Co., ISBN 044-4110-05-4, Amsterdam

Seraphin, B. O. (1976b). Chemical vapor deposition of thin semiconductor films for solar energy conversion. *Thin Solid Films*, Vol. 57, pp. 87- 94, ISSN 0040-6090

Siebers, D. L. & Kraabel, J. S. (1984). Estimating convective energy losses from solar central receivers. *Sandia Laboratory Report*, SAND84-8717

Singh, N.; Kaushik, S. C. & Misra R. D. (2000). Exergetic analysis of a solar thermal power system. *Renewable Energy*, Vol. 19, pp. 135-143, ISSN 0960-1481

Steinfeld, A. & Schubnell, M. (1993). Optimum aperture size and operating temperature of a solar cavity-receiver. *Solar Energy*, Vol. 50, pp. 19-25, ISSN 0038-092X

Tabor, H. (1958). Solar energy research: Program in the new desert research institute in Beersheba. *Solar Energy*, Vol. 2, pp. 3-6, ISSN 0038-092X

Taragan, E. (1999). A multistage solar receiver: the route to high temperature. *Solar Energy*, Vol. 67, pp. 3-11, ISSN 0038-092X

Taumoefolau, T.; Paitoonsurikarn, S.; Hughes, G. & Lovegrove, K. (2004). Experimental investigation of natural convection heat loss from a model solar concentrator cavity receiver. *Journal of Solar Energy Engineering*, Vol. 126, pp. 801-807, ISSN 0199-6231

Trieb, F. & Nitsch, J. (1998). Recommendations for the market introduction of solar thermal power stations. *Renewable Energy*, Vol. 14, pp. 17-22, ISSN 0960-1481

Wu, S. Y.; Xiao, L.; Cao, Y. D. & Li, Y. R. (2010). Convection heat loss from cavity receiver in parabolic dish solar thermal power system: A review. *Solar Energy*, Vol. 84, pp. 1342-1355, ISSN 0038-092X

Zarza, E.; Valenzuela, L.; Leon, J.; Hennecke, K.; Eck, M.; Weyers, H. D. & Eickhoff, M. (2004). Direct steam generation in parabolic troughs: Final results and conclusions of the DISS project. *Energy*, Vol. 29, pp. 635-644, ISSN 0360-5442

Zavoico, A. B. (2001). Solar power tower design basis document, Revision 0. *Sandia National Laboratories Report*, SAND2001-2100

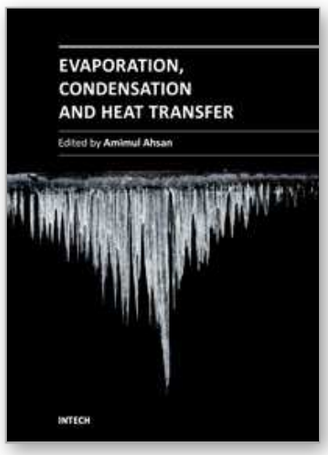

Evaporation, Condensation and Heat transfer
Edited by Dr. Amimul Ahsan

ISBN 978-953-307-583-9
Hard cover, 582 pages
Publisher InTech
Published online 12, September, 2011
Published in print edition September, 2011

The theoretical analysis and modeling of heat and mass transfer rates produced in evaporation and condensation processes are significant issues in a design of wide range of industrial processes and devices. This book includes 25 advanced and revised contributions, and it covers mainly (1) evaporation and boiling, (2) condensation and cooling, (3) heat transfer and exchanger, and (4) fluid and flow. The readers of this book will appreciate the current issues of modeling on evaporation, water vapor condensation, heat transfer and exchanger, and on fluid flow in different aspects. The approaches would be applicable in various industrial purposes as well. The advanced idea and information described here will be fruitful for the readers to find a sustainable solution in an industrialized society.

INTECH
open science | open minds

InTech Europe
University Campus STeP Ri
Slavka Krautzeka 83/A
51000 Rijeka, Croatia
Phone: +385 (51) 770 447
Fax: +385 (51) 686 166
www.intechopen.com

InTech China
Unit 405, Office Block, Hotel Equatorial Shanghai
No.65, Yan An Road (West), Shanghai, 200040, China
中国上海市延安西路65号上海国际贵都大饭店办公楼405单元
Phone: +86-21-62489820
Fax: +86-21-62489821

IntechOpen